# Advancements in Boron Difluoride Formazanate Dyes for Biological Imaging

**Shudan Yang**[1], **Kang Lu**[1], **Han Xiao**[1,2,3,4,*]

[1]Department of Chemistry, Rice University, 6100 Main Street, Houston, Texas, 77005

[2]SynthX Center, Rice University, 6100 Main Street, Houston, Texas, 77005

[3]Department of Biosciences, Rice University, 6100 Main Street, Houston, Texas, 77005

[4]Department of Bioengineering, Rice University, 6100 Main Street, Houston, Texas, 77005

## Abstract

In the past decade, boron difluoride formazanate dyes have gained considerable attraction due to their redox activity, high absorption and emission intensities, chemical stability across a broad range of conditions, and the ease to fine-tune their optical and electronic characteristics. Over the past five years, a boron difluoride formazanate dyes have demonstrated their extended emission wavelengths in the near-infrared region, suggesting their potential applications in the field of biological imaging. This review provides an overview of the evolution of boron difluoride formazanate dyes, encompassing the structural variations and corresponding optical properties, while also highlighting their current applications in biological imaging fields.

## 1. Introduction

Over the past decade, fluorescent dyes have attracted interest from scientists across a growing array of disciplines. These dyes have emerged as essential and invaluable tools in various fields of modern science and medicine. The advancements in modern fluorescent microscopy and imaging devices in recent years have further fueled enthusiasm for the development of next-generation imaging probes.

Among highly fluorescent dyes, the boron-difluoride chelating dye boron-dipyrromethene (BODIPY) stands out for its high quantum yield despite its short Stokes shift. However, boron difluoride ($BF_2$) formazanate dyes represent a novel class of probes for cell imaging and analyte sensing, characterized by their highly delocalized π-electron systems and large Stokes shift (Table 1). While the backbone of formazanate dyes had already been reported since 1890s[1], the early studies mainly focused on the coordination chemistry because of its special frontier molecular orbitals[2–15]. Despite the advancement of formazanate chemistry during this period, the potential applications of formazanate-metal complexes were hindered by their pronounced reactivity, limited stability, and significant high bio-toxicity[16–18]. In

---

[*]To whom correspondence should be addressed. han.xiao@rice.edu.
[§]These authors contributed equally

contrast to metal-based ligands, boron complexes featuring chelating nitrogen-donor ligands have garnered extensive attention as functional materials due to their remarkable chemical stability and potential for reduced biotoxicity.

Since the first $BF_2$ formazanate dye (**1, 2, and 5 of** Table 2) was reported in 2014[19], substantial efforts have been dedicated to enhancing its physical and near-infrared (NIR) optical properties. The growing interest in dyes that operate within the NIR region is due to the well-recognized "biological window" spanning from 650 to 1000 nm. This region offers several advantages, including reduced absorption and fluorescence signal interference from tissues or cells, decreased scattering, and improved tissue penetration depth[21–23]. These benefits, coupled with advancements in affordable NIR excitation sources and detectors, have spurred scientists to explore and engineer new fluorophores or fluorescent materials with superior molar absorption coefficients and enhanced fluorescence quantum yields.

In 2018, the first NIR $BF_2$ formazanate dye (**21** of Table 2) was introduced[20]. Since that breakthrough, $BF_2$ formazanate dyes have captured the attention of both biochemists and biologists, steadily gaining popularity as promising candidates for NIR fluorescent probes. While cyanine and BODIPY have traditionally served as the primary platforms for NIR dyes, they both have inherent limitations. Cyanine structures are susceptible to rotational and photoisomerization events in their flexible bonds, often leading to nonradiative deactivation pathways. On the other hand, the synthesis of BODIPY dyes faces challenges in achieving significant red shifts in absorption and emission maxima through large aromatic ring substitutions. In contrast, the structural rigidity, high chemical stability, and the "three-in-one" synthetic approach (Figure 1A) in the synthesis of $BF_2$ formazanate dyes facilitate the expansion of their structural versatility, making them well-suited for applications in fluorescent sensors, bio-imaging, and more.

In this review, we provide an overview of the optical characteristics of reported $BF_2$ formazanate dyes. Our analysis delves into the intricate structure-property relationships, exploring their impact on the absorption, emission, molar absorption coefficients, and fluorescent quantum yields of $BF_2$ formazanate dyes. This in-depth examination will serve as a valuable resource for guiding the future design of NIR-I/II $BF_2$ formazanate dyes. Furthermore, we review the biological imaging applications of the $BF_2$ formazanate dyes that have been explored to date.

## 2.  Optical Properties of Boron Difluoride Formazanate Dyes

In contrast to other $BF_2$ chelating complexes such as BODIPY, where the tricycle ring is rigidly flattened into a plane by the boron atom, forming an integrated heteroaromatic system[24–26]. X-ray crystallography analysis reveals that in the solid phase, $BF_2$ formazanates adopt a somewhat "dragonfly" conformation. The four coordinated boron atoms, which binds to the formazanate backbone through two nitrogen atoms, slightly displace from the formazanate backbone by 0.19 Å in Figure 1B (**2**) and 0.46 Å in Figure 1B (**3**), resulting in a delocalized formazanate structure. The nitrogen–nitrogen and carbon–nitrogen bond lengths of the formazanate ligand backbone falling between the typical values associated with single and double bonds of the same atoms. In most

cases, the nitrogen-nitrogen bond lengths are in the range of 1.29–1.31 Å, and the carbon-nitrogen bond lengths are in 1.33–1.36 Å.[19,27–29] Moreover, through computational studies employing DFT calculations of the frontier molecular orbitals shown in Figure 1B, both LUMOs and HOMOs orbitals are highly delocalized over the formazanate backbone and N-aryl substituents for each structure. While it is evident that R3 substituents predominantly influence the HOMOs due to the presence of a nodal plane, whereas N-aryl substituents (R1 and R2) are expected to have a more substantial impact on the LUMOs. In addition, DFT calculations also showed that the HOMO of (**1**) is highly delocalized and includes significant orbital density on the phenyl ring appended to the carbon of the formazanate backbone. The energy gap between HOMO-LUMO pair of Figure 1B (**1**) corresponds to its lowest excitation energy and longer absorption and emission wavelength compared to (**2**) and (**3**).[29–31] Consequently, the optical properties of $BF_2$ formazanate dyes are intricately linked to factors such as $\pi$-conjugation, torsion angles, and the electronic characteristics of the $R_1$, $R_2$, and $R_3$ substituents.

### 2.1. $R_3$ substituents

Since $R_3$-substituents only affect the HOMO orbital, their influence on maximum absorption and emission is comparatively weaker when compared to N-substitution or $\pi$-conjugation. When $R_3$ is a strong electron-withdrawing group, such as cyano or nitro (**14** or **16** of Table 2), its absorption wavelength tends to be slightly longer than that of $R_3$ as a weak electron-withdrawing or electron-donating group (**15** of Table 2), mainly due to electrochemical reduction potentials. When compared to cyano or nitro substitution at $R_3$ position, 3-phenyl formazanates consistently exhibit greater stokes shifts and maximum emission due to larger conjugation system. However, the fluorescence quantum yields of triarylformazanates are typically quite low, often falling below 0.01 in either polar or nonpolar solvents. This phenomenon can be attributed to an increased prevalence of non-radiative decay processes, likely associated with the vibrational and/or free rotational motions of the 3-aryl substituents.[28,29]

### 2.2. *N*-aryl substituents

Addition of electron-donating group at the *meta*- or *para*- position of the N-aryl substituents can lead to a significant red-shift and enhancement of absorption and photoluminescence spectra of $BF_2$ formazanate dyes. This effect can be attributed to the intramolecular charge transfer (ICT) between the donor (EDG group) and acceptor ($BF_2$ formazanate backbone) characteristics. The great movement of electrons from electron donor to the electron deficient $BF_2$ formazanate backbone typically results in long wavelength and strong fluorescence intensity. Additionally, the extended electron pair of the EDG group can participate in the delocalization within the $\pi$-conjugating system, potentially contributing to a degree of planar conjugation formazanate network. Somewhat paradoxically, N-aryl substituents featuring electron-withdrawing groups (such as cyano groups[19,30] or triple bonds[32,33]) at the *para*-position also result in a slight red-shift in the UV/Vis and emission spectra. To decipher the underlying mechanism of this phenomenon, molecular orbitals and the lowest electronic excitation energies of these compounds were computed using density functional theory (DFT) methods. The study demonstrated that the incorporation of an N-aryl ring with electron-withdrawing groups, such as a cyano group or triple bond,

increases the spatial extent of π-conjugation within the molecule. Consequently, this lowers the energy of the π→π* transition, leading to the observed red-shift in the UV absorption band.[19] However, the later study suggests that the EDG group with the longer pair can significantly extend both absorption and emission into the NIR-I or -II regions.

Despite persistent efforts to expand the absorption and emission wavelengths of $BF_2$ formazanate dyes, they had remained confined to the visible light region. However, in 2018, a breakthrough was achieved by introducing a *p*-dimethylamine substituent on the *N*-aryl of the $BF_2$ formazanate structure[20] (**21** of Table 2). This modification extended the fluorescence of this dye series into the near-infrared region, exhibiting photoluminescence ranging from 750 nm to 1050 nm, thus paving the way for potential biological applications. The dimethylaminophenyl group demonstrated significantly superior electron-donating capacity when compared to the methoxyphenyl group, and X-ray crystallography revealed a quinoidal character resulting from bond alterations. This quinoidal character proved to be critical for the dramatic redshift observed in the $BF_2$ formazanate dyes.

In 2020, Pt (II)-acetylides were incorporated into the *N*-aryl substituents, elongating the electronic conjugation via triple bonds and shifting the absorption and emission maxima of $BF_2$ formazanate dyes to 650-700 nm and 750-800 nm, respectively. Nevertheless, the introduction of Pt (II) notably diminished the fluorescence quantum yield of the conjugated formazanate dye to below 0.01.[32,34] To further augment the π-conjugation system, within the same year, *p*-diphenylamine was introduced onto *N*-aryl substituents (**23, 24** of Table 2), thereby expanding the maximum absorption to approximately 750 nm and emission to beyond 900 nm.[35] Despite the spectral red shift, the incorporation of the *N*-aryl substituent led to a significant decrease in quantum yield, likely attributed to enhanced non-radiative decay processes.

In 2022, a range of 3-cyanoformazanate dyes featuring diverse electron-donating *N*-aryl substituents were developed (**25 – 30** of Table 2), showing adjustable photophysical characteristics, exceptional photostability, robust biological stability, and intense luminescence. N-aryl substituents have significant quinoidal character, which enables narrowing the energy gap and dramatically extends the π-system to enhance electron delocalization. The authors therefore altered the electron-rich π-conjugated system at the N-1,3 position substituents with different nitrogen-containing rings (from aziridine to julolidine) to optimize the photophysical profiles of these $BF_2$ formazanate dyes. In the investigation, the emission of these $BF_2$ formazanate dyes was extended into the NIR-II window. This spectral region is characterized by minimal photon scattering and autofluorescence, rendering it particularly advantageous for deep-tissue bioimaging. Notably, formazanate dyes with morpholine substitution demonstrated a notable ability to traverse the blood-brain barrier (BBB) *in vivo*.[36]

### 2.3. Dimer, oligomer and polymer

Besides modifications at the $R_1$, $R_2$, and $R_3$ positions, recent studies have explored the conjugation of the $BF_2$ formazanate backbone into dimers, trimers, or larger polymers. In 2015, *meta*- (**17** of Table 2) and para- (**18** of Table 2) substituted benzene-bridged $BF_2$ formazanate dimers were among the pioneering examples. The para-conformer, in particular,

exhibited redshifted absorption and emission maxima compared to its monomer.[38] Since 2020, $BF_2$ formazanates have been employed as monomers with various moieties in polymer design, leading to a wide range of electrochemical and optical properties. This expansion significantly broadened the scope of $BF_2$ formazanate chemistry.[39–43]

## 3. Biological Imaging Applications of Boron Difluoride Formazanate Dyes

Due to their structural diversity, high biocompatibility, and tunable photophysical properties, $BF_2$ formazanate dyes have recently found utility in various chemical and biological applications.

### 3.1. pH sensor

The potential of $BF_2$ formazanate dyes as building blocks for pH indicators was first demonstrated in 2017, employing a 2-pyridyl substituent at the $R_3$ position of the formazanate backbone. In a neutral environment, the free rotation of the pyridine moiety led to fluorescence quenching through non-radiative energy decay, resulting in fluorescence quantum yields ($\Phi_F$) of less than 1% in $CH_2Cl_2$. However, upon protonation occurring at pH levels below 4, an increase in fluorescence intensity, accompanied by a slight redshift, was observed. The maximum reported $\Phi F$ reached 18% as reported (Figure 2A).[45]

### 3.2. Cell imaging

The first $BF_2$ formazanate dye utilized in cell imaging, *p*-anisole-3-cyanoformazanate (**5** of Table 2), was reported in 2015 for its robust deep red fluorescence intensity.[28] Following this, in 2017, tetraethylene glycol (TEG)-functionalized $BF_2$ complexes of 3-cyanoformazanates were introduced. The incorporation of solubilizing TEG chains at the *N*-aryl substituents not only significantly enhanced the water solubility of $BF_2$ formazanate dyes but also extended the dye's emission into the near-infrared region. This amphiphilic probe was utilized for imaging mouse fibroblast cells.[33] In 2020, an asymmetrical $BF_2$ formazanate dye was linked to peptides with notable binding affinity for modified growth hormone secretagogue receptor (GHSR-1a) or gastrin releasing peptide receptor (GRPR) through a click reaction. This was the first endeavor to conjugate a $BF_2$ formazanate dye onto either the C- or N-terminal regions of short peptides and demonstrated its feasibility for targeted imaging (Figure 2B).[46]

### 3.3. Photoacoustic and NIR imaging for deep tissues

In 2021, significant progress was made with NIR-II organic nanoparticles formed through the self-assembly of a $BF_2$ formazanate dye with an amphiphilic polymer. These nanoparticles have shown promising potential as highly efficient phototheranostic agents within the NIR-II biological window. Thanks to strong $\pi$–$\pi$ stacking interactions, they exhibit a broad absorption spectrum in the second near-infrared region, ranging from 900 nm to 1200 nm, enabling robust photoacoustic (PA) imaging capabilities (Figure 2C).[47]

Building upon the exceptional performance of $BF_2$ formazanate nanoparticles in phototheranostic applications, two additional $BF_2$ formazanate dyes (**23, 31** of Table 2) were synthesized in 2022 specifically for NIR-II fluorescence imaging-guided cancer therapy. A

novel small molecular fluorescent dye for NIR-II imaging, BDF-Ph (**23** of Table 2), was developed by incorporating electron-rich triphenylamine units onto the $BF_2$ formazanate scaffold, emitting at 975 nm with a high fluorescence quantum yield. This resulting $BF_2$ formazanate dye was encapsulated within amphiphilic polystyrene-g-poly (ethylene glycol) to yield NIR-II $BF_2$ formazanate nanoparticles. *In vivo* studies demonstrated strong NIR-II fluorescence signals.[48] Additionally, BDF1005, another molecular NIR-II dye with a structure similar to BDF-Ph but possessing a larger π-conjugation system, exhibited a redshifted absorption at 768 nm and a NIR-II peak emission at 1034 nm. Both *in vitro* and *in vivo* experiments showcased the potential of BDF1005-based nanotheranostics for NIR-II fluorescence imaging-guided therapy.[37]

### 3.4. Blood–brain barrier crossing and brain imaging

The blood-brain barrier (BBB) serves as a formidable barrier, largely preventing the entry of molecules into the central nervous system, particularly those with significant molecular weights. This characteristic poses a challenge for the utilization of NIR-II dyes in noninvasive brain imaging, as they typically possess large molecular frameworks. In 2022, a novel series of NIR-II dyes, based on the comparatively smaller scaffold of $BF_2$ formazanates, was developed, allowing their passage across the BBB for noninvasive brain imaging[36].

This advancement was achieved through strategic modifications to the aniline moiety of $BF_2$ formazanate dyes, resulting in an extension of their absorption and emission wavelengths. Additionally, the incorporation of a morpholine group markedly enhanced their capacity to traverse the BBB. Subsequently, these $BF_2$-formazanate dyes were utilized for imaging intact mouse brains and monitoring the dynamic diffusion of the dye across the BBB in the NIR-II region. Furthermore, using murine glioblastoma models, these dyes demonstrated the ability to distinguish tumors from normal brain tissues. This discovery underscores the potential of this series of molecules in the development of probes and drugs relevant to theranostics for brain pathologies (Figure 2D).[36]

## 4. Conclusion and perspectives

This review provides an overview of the advancements in $BF_2$ formazanate dyes, highlighting their superiority over other NIR-I/II dyes due to their small size, ideal lipophilicity, low polar surface areas, tunable photophysical properties, ultrahigh photostability[36], and excellent biological stability—critical parameters for in vivo deep tissue imaging. While recent years have seen progress in designing new $BF_2$ formazanate structures, the focus has primarily been on their electronic, optical, and redox properties, with limited applications in the biomedical field. Given the exceptional flexible fluorophore platform offered by $BF_2$ formazanates, this review aims to inspire rational design and the creation of functional $BF_2$ formazanate probes for chemical and biological applications, with the potential for significant biomedical utility *in vivo*.

## Acknowledgements

## 5. Reference

(1). Nineham AW The Chemistry of Formazans and Tetrazolium Salts. Chem. Rev 1955, 55 (2), 355–483. 10.1021/cr50002a004.

(2). Barbon SM; Staroverov VN; Gilroy JB Structurally Diverse Boron–Nitrogen Heterocycles from an $N_2O_2^{3-}$ Formazanate Ligand. Angew. Chem. Int. Ed 2017, 56 (28), 8173–8177. 10.1002/anie.201704285.

(3). Gilroy JB; Patrick BO; McDonald R; Hicks RG Transition Metal Complexes of 3-Cyano- and 3-Nitroformazans. Inorg. Chem 2008, 47 (4), 1287–1294. 10.1021/ic7019846. [PubMed: 18211010]

(4). Maar RR; Catingan SD; Staroverov VN; Gilroy JB Formazanate Complexes of Hypervalent Group 14 Elements as Precursors to Electronically Stabilized Radicals. Angew. Chem. Int. Ed 2018, 57 (31), 9870–9874. 10.1002/anie.201806097.

(5). Mondol R; Otten E Aluminum Complexes with Redox-Active Formazanate Ligand: Synthesis, Characterization, and Reduction Chemistry. Inorg. Chem 2019, 58 (9), 6344–6355. 10.1021/acs.inorgchem.9b00553. [PubMed: 30978008]

(6). Maar RR; Rabiee Kenaree A; Zhang R; Tao Y; Katzman BD; Staroverov VN; Ding Z; Gilroy JB Aluminum Complexes of $N_2O_2^{3-}$ Formazanate Ligands Supported by Phosphine Oxide Donors. Inorg. Chem 2017, 56 (20), 12436–12447. 10.1021/acs.inorgchem.7b01907. [PubMed: 28960966]

(7). Milocco F; Demeshko S; Meyer F; Otten E Ferrate( II ) Complexes with Redox-Active Formazanate Ligands. Dalton Trans. 2018, 47 (26), 8817–8823. 10.1039/C8DT01597J. [PubMed: 29922783]

(8). Travieso-Puente R; Broekman JOP; Chang M-C; Demeshko S; Meyer F; Otten E Spin-Crossover in a Pseudo-Tetrahedral Bis(Formazanate) Iron Complex. J. Am. Chem. Soc 2016, 138 (17), 5503–5506. 10.1021/jacs.6b01552. [PubMed: 27074728]

(9). Kabir E; Mu G; Momtaz DA; Bryce NA; Teets TS Formazanate Complexes of Bis-Cyclometalated Iridium. Inorg. Chem 2019, 58 (17), 11672–11683. 10.1021/acs.inorgchem.9b01657. [PubMed: 31430140]

(10). Mandal A; Schwederski B; Fiedler J; Kaim W; Lahiri GK Evidence for Bidirectional Noninnocent Behavior of a Formazanate Ligand in Ruthenium Complexes. Inorg. Chem 2015, 54 (16), 8126–8135. 10.1021/acs.inorgchem.5b01408. [PubMed: 26244848]

(11). Milocco F; De Vries F; Dall'Anese A; Rosar V; Zangrando E; Otten E; Milani B Palladium Alkyl Complexes with a Formazanate Ligand: Synthesis, Structure and Reactivity. Dalton Trans. 2018, 47 (41), 14445–14451. 10.1039/C8DT03130D. [PubMed: 30183797]

(12). Chang M; Dann T; Day DP; Lutz M; Wildgoose GG; Otten E The Formazanate Ligand as an Electron Reservoir: Bis(Formazanate) Zinc Complexes Isolated in Three Redox States. Angew. Chem. Int. Ed 2014, 53 (16), 4118–4122. 10.1002/anie.201309948.

(13). Khan SA; Shahid S; Kanwal S; Rizwan K; Mahmood T; Ayub K Synthesis of Novel Metal Complexes of 2-((Phenyl (2-(4-Sulfophenyl) Hydrazono) Methyl) Diazenyl) Benzoic Acid Formazan Dyes: Characterization, Antimicrobial and Optical Properties Studies on Leather. J. Mol. Struct 2019, 1175, 73–89. 10.1016/j.molstruc.2018.07.081.

(14). Milocco F; De Vries F; Bartels IMA; Havenith RWA; Cirera J; Demeshko S; Meyer F; Otten E Electronic Control of Spin-Crossover Properties in Four-Coordinate Bis(Formazanate) Iron(II) Complexes. J. Am. Chem. Soc 2020, 142 (47), 20170–20181. 10.1021/jacs.0c10010. [PubMed: 33197175]

(15). Jin D; Sun X; Hinz A; Roesky PW Rare-Earth Metal Complexes with Redox-Active Formazanate Ligands. Dalton Trans. 2022, 51 (13), 5218–5226. 10.1039/D2DT00456A. [PubMed: 35275153]

(16). Frath D; Massue J; Ulrich G; Ziessel R Luminescent Materials: Locking π-Conjugated and Heterocyclic Ligands with Boron(III). Angew. Chem. Int. Ed 2014, 53 (9), 2290–2310. 10.1002/anie.201305554.

(17). Araneda JF; Piers WE; Heyne B; Parvez M; McDonald R High Stokes Shift Anilido-Pyridine Boron Difluoride Dyes. Angew. Chem. Int. Ed 2011, 50 (51), 12214–12217. 10.1002/anie.201105228.

(18). Tamgho I-S; Hasheminasab A; Engle JT; Nemykin VN; Ziegler CJ A New Highly Fluorescent and Symmetric Pyrrole–BF2 Chromophore: BOPHY. J. Am. Chem. Soc 2014, 136 (15), 5623–5626. 10.1021/ja502477a. [PubMed: 24707882]

(19). Barbon SM; Reinkeluers PA; Price JT; Staroverov VN; Gilroy JB Structurally Tunable 3-Cyanoformazanate Boron Difluoride Dyes. Chem. – Eur. J 2014, 20 (36), 11340–11344. 10.1002/chem.201404297. [PubMed: 25066035]

(20). Maar RR; Zhang R; Stephens DG; Ding Z; Gilroy JB Near-Infrared Photoluminescence and Electrochemiluminescence from a Remarkably Simple Boron Difluoride Formazanate Dye. Angew. Chem. Int. Ed 2019, 58 (4), 1052–1056. 10.1002/anie.201811144.**As the first time that the emission of BF$_2$ formazanate dyes being extended to the NIR region, this article endowed this sort of dyes broader application in chemical and biological area and remarkable performance in theranostic imaging.

(21). Weissleder R A Clearer Vision for in Vivo Imaging. Nat. Biotechnol 2001, 19 (4), 316–317. 10.1038/86684. [PubMed: 11283581]

(22). Frangioni JV In Vivo Near-Infrared Fluorescence Imaging. Curr. Opin. Chem. Biol 2003, 7 (5), 626–634. 10.1016/j.cbpa.2003.08.007. [PubMed: 14580568]

(23). Thimsen E; Sadtler B; Berezin MY Shortwave-Infrared (SWIR) Emitters for Biological Imaging: A Review of Challenges and Opportunities. Nanophotonics 2017, 6 (5), 1043–1054. 10.1515/nanoph-2017-0039.

(24). Boens N; Leen V; Dehaen W Fluorescent Indicators Based on BODIPY. Chem. Soc. Rev 2012, 41 (3), 1130–1172. 10.1039/C1CS15132K. [PubMed: 21796324]

(25). Lu H; Mack J; Yang Y; Shen Z Structural Modification Strategies for the Rational Design of Red/NIR Region BODIPYs. Chem. Soc. Rev 2014, 43 (13), 4778–4823. 10.1039/C4CS00030G. [PubMed: 24733589]

(26). Ulrich G; Ziessel R; Harriman A The Chemistry of Fluorescent Bodipy Dyes: Versatility Unsurpassed. Angew. Chem. Int. Ed 2008, 47 (7), 1184–1201. 10.1002/anie.200702070.

(27). Lide DR; Baysinger G; Chemistry S; Berger LI; Goldberg RN; Kehiaian HV CRC Handbook of Chemistry and Physics.

(28). Maar RR; Barbon SM; Sharma N; Groom H; Luyt LG; Gilroy JB Evaluation of Anisole-Substituted Boron Difluoride Formazanate Complexes for Fluorescence Cell Imaging. Chem. – Eur. J 2015, 21 (44), 15589–15599. 10.1002/chem.201502821. [PubMed: 26397738]

(29). Barbon SM; Staroverov VN; Gilroy JB Effect of Extended π Conjugation on the Spectroscopic and Electrochemical Properties of Boron Difluoride Formazanate Complexes. J. Org. Chem 2015, 80 (10), 5226–5235. 10.1021/acs.joc.5b00620. [PubMed: 25944006]

(30). Barbon SM; Price JT; Reinkeluers PA; Gilroy JB Substituent-Dependent Optical and Electrochemical Properties of Triarylformazanate Boron Difluoride Complexes. Inorg. Chem 2014, 53 (19), 10585–10593. 10.1021/ic5016912. [PubMed: 25226240]

(31). Gilroy JB; Otten E Formazanate Coordination Compounds: Synthesis, Reactivity, and Applications. Chem. Soc. Rev 2020, 49 (1), 85–113. 10.1039/C9CS00676A. [PubMed: 31802081]

(32). Dhindsa JS; Melenbacher A; Barbon SM; Stillman MJ; Gilroy JB Altering the Optoelectronic Properties of Boron Difluoride Formazanate Dyes via Conjugation with Platinum( ɪɪ )-Acetylides. Dalton Trans. 2020, 49 (45), 16133–16142. 10.1039/C9DT03417J. [PubMed: 31599277]

(33). Barbon SM; Novoa S; Bender D; Groom H; Luyt LG; Gilroy JB Copper-Assisted Azide–Alkyne Cycloaddition Chemistry as a Tool for the Production of Emissive Boron Difluoride 3-Cyanoformazanates. Org. Chem. Front 2017, 4 (2), 178–190. 10.1039/C6QO00640J.*

Asymmetric BF$_2$ formazanate dye was developed with alkyn group, which makes the subcellular targeting image with this sort of dyes being possible.

(34). Dhindsa JS; Maar RR; Barbon SM; Avilés MO; Powell ZK; Lagugné-Labarthet F; Gilroy JB A π-Conjugated Inorganic Polymer Constructed from Boron Difluoride Formazanates and Platinum(II) Diynes. Chem. Commun 2018, 54 (50), 6899–6902. 10.1039/C8CC02424C.

(35). Buguis FL; Maar RR; Staroverov VN; Gilroy JB Near-Infrared Boron Difluoride Formazanate Dyes. Chem. – Eur. J 2021, 27 (8), 2854–2860. 10.1002/chem.202004793. [PubMed: 33140465]

(36). Wang S; Shi H; Wang L; Loredo A; Bachilo SM; Wu W; Tian Z; Chen Y; Weisman RB; Zhang X; Cheng Z; Xiao H Photostable Small-Molecule NIR-II Fluorescent Scaffolds That Cross the Blood–Brain Barrier for Noninvasive Brain Imaging. J. Am. Chem. Soc 2022, 144 (51), 23668–23676. 10.1021/jacs.2c11223. [PubMed: 36511618] **In this article developed novel BF$_2$ formazanate dyes, exhibiting longer fluorescence in NIR-II region and outstanding capacity of Blood–brain barrier crossing, were first reported. These progress underscores the potential of this series molecuels in the utilization of probes or drugs for brain pathologies.

(37). Dai H; Cheng Z; Zhang T; Wang W; Shao J; Wang W; Zhao Y; Dong X; Zhong L Boron Difluoride Formazanate Dye for High-efficiency NIR-II Fluorescence Imaging-guided Cancer Photothermal Therapy. Chin. Chem. Lett 2022, 33 (5), 2501–2506. 10.1016/j.cclet.2021.11.079.

(38). Barbon SM; Price JT; Yogarajah U; Gilroy JB Synthesis and Characterization of Conjugated/Cross-Conjugated Benzene-Bridged Boron Difluoride Formazanate Dimers. RSC Adv. 2015, 5 (69), 56316–56324. 10.1039/C5RA09505K.

(39). Dhindsa JS; Cotterill EL; Buguis FL; Anghel M; Boyle PD; Gilroy JB Blending the Optical and Redox Properties of Oligoynes and Boron Difluoride Formazanates. Angew. Chem. Int. Ed 2022, 61 (39), e202208502. 10.1002/anie.202208502.

(40). Kumar C; Agrawal AR; Ghosh NG; Karmakar HS; Das S; Kumar NR; Banewar VW; Zade SS Boron Difluoride Formazanates with Thiophene and 3,4-Ethylenedioxythiophene Capping and Their Electrochemical Polymerization. Dalton Trans. 2020, 49 (38), 13202–13206. 10.1039/D0DT02905J. [PubMed: 32966457]

(41). Kawano Y; Ito Y; Ito S; Tanaka K; Chujo Y π-Conjugated Copolymers Composed of Boron Formazanate and Their Application for a Wavelength Converter to Near-Infrared Light. Macromolecules 2021, 54 (4), 1934–1942. 10.1021/acs.macromol.0c02315.

(42). Ito S; Ito Y; Kazuo T; Chujo Y Near-Infrared-Emissive π-Conjugated Polymers Based on Five-Coordinated Silicon Formazanate Complexes. Polymer 2022, 239, 124463. 10.1016/j.polymer.2021.124463.

(43). Buguis FL; Hsu NSY; Sirohey SA; Adam MC; Goncharova LV; Gilroy JB Dyads and Triads of Boron Difluoride Formazanate and Boron Difluoride Dipyrromethene Dyes. Chem. – Eur. J n/a (n/a), e202302548. 10.1002/chem.202302548.

(44). Ulrich G; Ziessel R; Harriman A The Chemistry of Fluorescent Bodipy Dyes: Versatility Unsurpassed. Angew. Chem. Int. Ed 2008, 47 (7), 1184–1201. 10.1002/anie.200702070.

(45). Barbon SM; Buddingh JV; Maar RR; Gilroy JB Boron Difluoride Adducts of a Flexidentate Pyridine-Substituted Formazanate Ligand: Property Modulation via Protonation and Coordination Chemistry. Inorg. Chem 2017, 56 (19), 12003–12011. 10.1021/acs.inorgchem.7b01984. [PubMed: 28921960]

(46). The development of peptide–boron difluoride formazanate conjugates as fluorescence imaging agents - RSC Advances (RSC Publishing). https://pubs.rsc.org/en/content/articlelanding/2020/ra/d0ra02104k#! (accessed 2023-12-02).

(47). Xiang H; Zhao L; Yu L; Chen H; Wei C; Chen Y; Zhao Y Self-Assembled Organic Nanomedicine Enables Ultrastable Photo-to-Heat Converting Theranostics in the Second near-Infrared Biowindow. Nat. Commun 2021, 12 (1), 218. 10.1038/s41467-020-20566-6. [PubMed: 33431882]

(48). Li H; Dai H; Mei A; Ruan X; Wang W; Yang D; Wang W; Zhang Q; Dong X; Shao J Triphenylamine Flanked Boron Difluoride Formazanate for NIR-II Fluorescence Imaging-Guided Photothermal Therapy. Dyes Pigments 2022, 205, 110478. 10.1016/j.dyepig.2022.110478.

(49). Chang MC; Chantzis A; Jacquemin D; Otten E Boron difluorides with formazanate ligands: redox-switchable fluorescent dyes with large stokes shifts. Dalton Transactions 2016, 23, 9477. 10.1039/C6DT01226D.
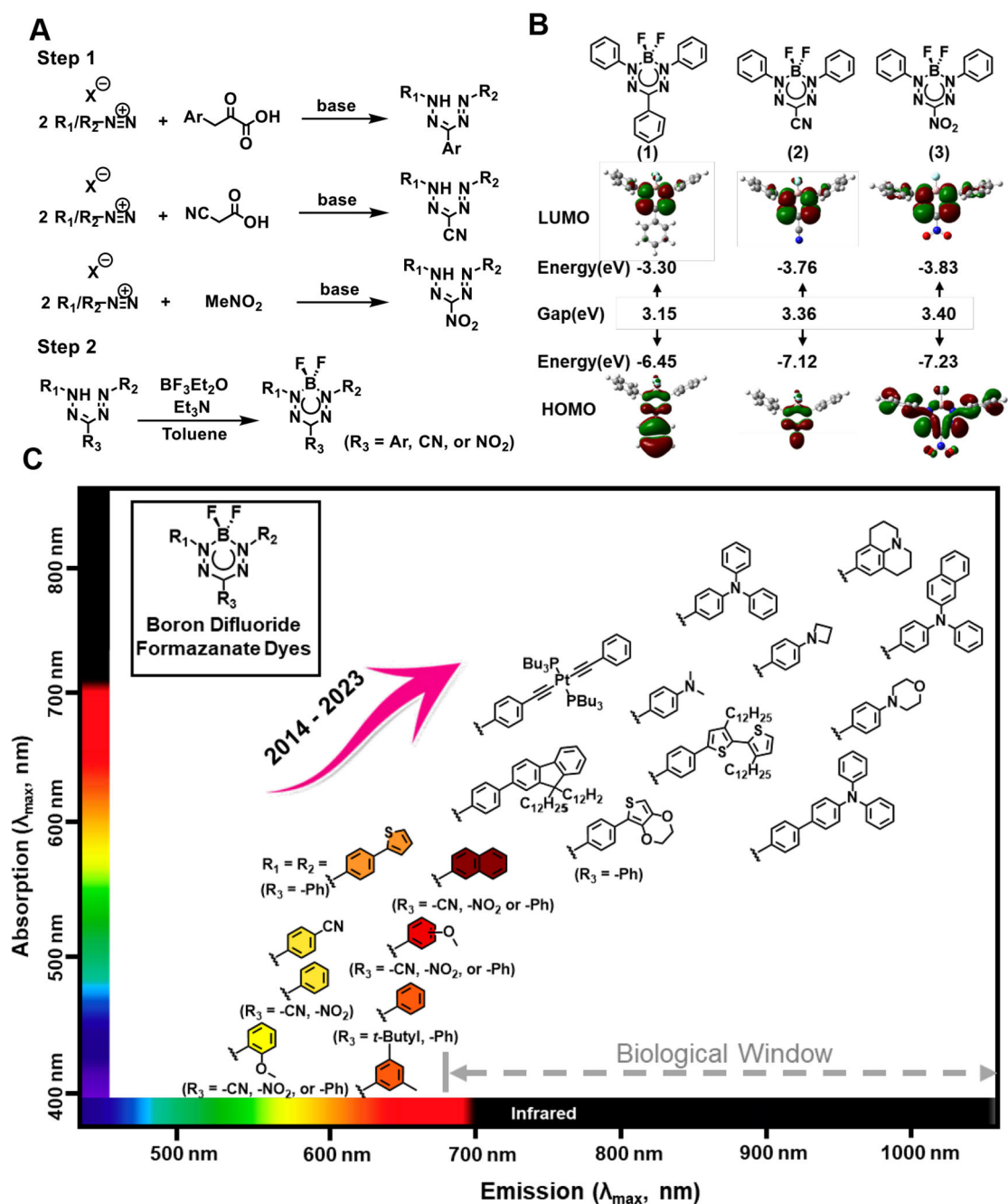
**Figure 1.**

(**A**) Common routes for the synthesis of formazans. (**B**) HOMOs and LUMOs calculated (DFT: B3LYP/6-311+G*) for toluene solutions of $BF_2$ complexes. (**C**) Absorption and emission properties of selected $BF_2$ formazanate dyes. $R_1$ and $R_2$ groups of formazanate dyes are shown in the graph. $R_3$ is default as cyano if without labeling.
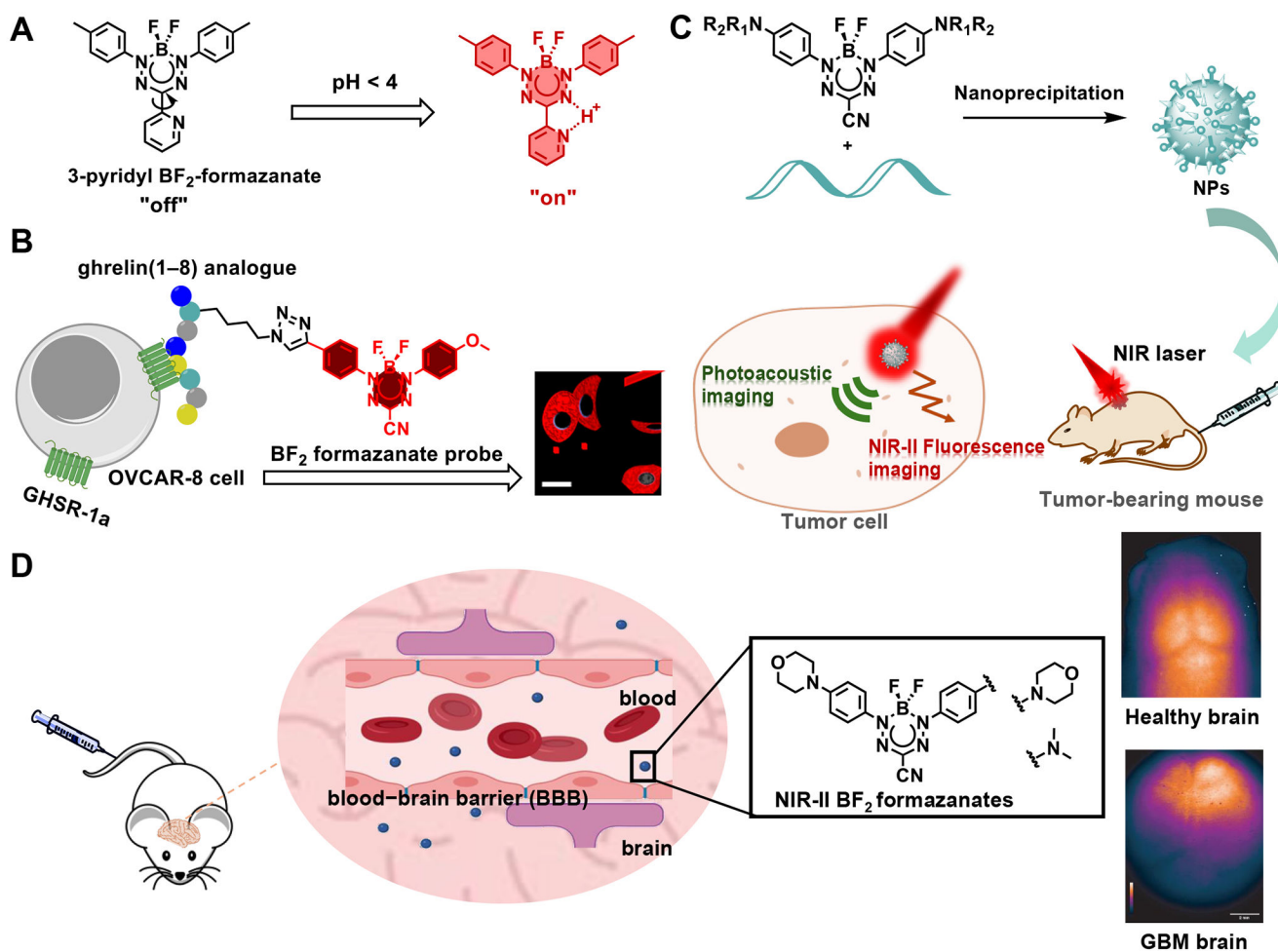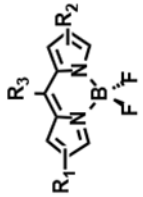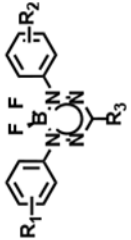
**Figure 2.**
Biological imaging of BF$_2$ formazanate dyes. **(A)** 3-pyridyl BF$_2$ formazanate was used
as pH sensor. **(B)** Asymmetrical BF$_2$ formazanate dye connected to GHSR-1a-targeting
peptide via click reaction and applied in cell imaging with confocal. **(C)** NIR-II organic
nanoparticles served as highly efficient phototheranostic agents in the NIR-II bio window.
**(D)** A series of novel BF$_2$ formazanate NIR-II dyes exhibited excellent blond-brain barrier
crossing capacity, which were used in brain imaging.

**Table 1.**

Comparison of BODIPY and BF$_2$ formazanate dyes

| Dye | Basic Structure | Photophysical Properties | Applications of Derivatives |
|---|---|---|---|
| **BODIPY** (First reported in 1968) | | $\lambda_{abs}$ = 500 nm $\lambda_{em}$ = 516 nm Stokes shift: 16 nm $\Phi_F$ = 0.77 (THF) | Fluorescence sensor Bioimaging Electrochemiluminescence |
| **BF$_2$ Formazanate** (First reported in 2014) | | $\lambda_{abs}$ = 489 nm $\lambda_{em}$ = 585 nm Stokes shift: 96 nm $\Phi_F$ = 0.05 (THF) | Fluorescence sensor NIR-II Bioimaging Electrochemiluminescence |
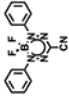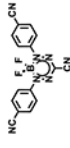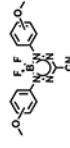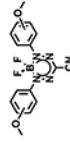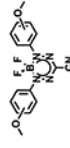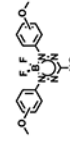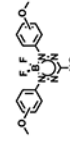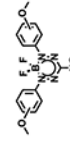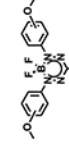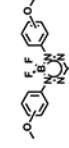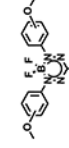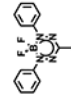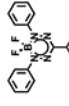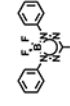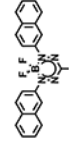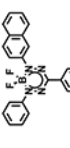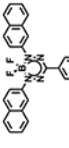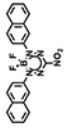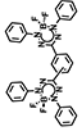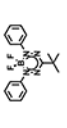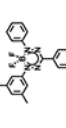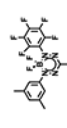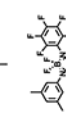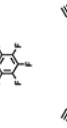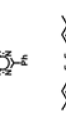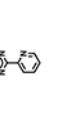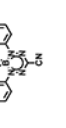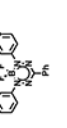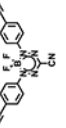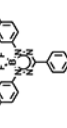
**Table 2.**

Spectroscopic data for selected BF$_2$ formazanate dyes

| BF$_2$-formazanate | $\lambda_{abs}$ (nm) | $\varepsilon$ (*10$^4$ M$^{-1}$ cm$^{-1}$) | $\lambda_{em}$ (nm) | $\Phi$ | Year |
|---|---|---|---|---|---|
| 1[a] | 491 | 3.46 | 584 | 0.09 | 2014[19] |
| 2[a] | 499 | 2.24 | 589 | 0.17 | 2014[19] |
| 3[a] (o) | 466 (o) | 1.55 (o) | 589 (o) | 0.04 (o) | 2014[19,28] |
| 4[a] (m) | 517 (m) | 1.85 (m) | 637 (m) | 0.03 (m) | |
| 5[a] (p) | 558 (p) | 3.53 (p) | 661 (p) | 0.65 (p) | |
| 6[a] (o) | 466 (o) | 0.71 (o) | 599 (o) | 0.03 (o) | |
| 7[a] (m) | 511 (m) | 1.83 (m) | 651 (m) | <0.01 (m) | 2015[28] |
| 8[a] (p) | 564 (p) | 2.01 (p) | 665 (p) | 0.24 (p) | |
| 9[a] (o) | 464 (o) | 2.16 (o) | 588 (o) | 0.01 (o) | |
| 10[a] (m) | 521 (m) | 2.50 (m) | 644 (m) | 0.03 (m) | 2015[28] |
| 11[a] (p) | 545 (p) | 2.93 (p) | 670 (p) | 0.06 (p) | |
| 12[a] | 509 | 2.34 | 630 | 0.01 | 2015[29] |
| 13[a] | 524 | 2.03 | 656 | 0.09 | 2015[29] |
| 14[a] | 488 | 2.92 | 587 | 0.03 | 2015[29] |
| 15[a] | 558 | 2.39 | 669 | 0.32 | 2015[29] |
| 16[a] | 530 | 2.75 | 656 | 0.03 | 2015[29] |
| 17[a] | 551 | 2.36 | 682 | <0.01 | 2015[29] |

| | | | | | |
|---|---|---|---|---|---|
| 18[a] |  | 563 | 2.67 | 677 | 0.28 | 2015[29] |
| 19[a] (m) / 20[a] (p) |  | 507 (m) / 523 (p) | 3.96 (m) / 3.09 (p) | 627 (m) / 654 (p) | 0.03 (m) / 0.08 (p) | 2015[38] |
| 21[b] |  | 473 | 1.32 | 643 | <0.1 | 2016[49] |
| 22[b] |  | 464 | 2.13 | 617 | <0.1 | 2016[49] |
| 23[b] |  | 460 | 1.21 | 610 | <0.1 | 2016[49] |
| 24[b] |  | 414 | 1.19 | 650 | <0.1 | 2016[49] |
| 25[a] |  | 530 | 3.27 | 635 | 0.18 | 2017[33] |
| 26[a] |  | 517 | 2.62 | 626 (pH 4) / 633 (pH 10) | 0.18 (pH 4) / 0.01 (pH 10) | 2017[46] |
| 27[a] |  | 733 | 4.13 | 866 | 0.04 | 2018[20] |
| 28[a] |  | 526 | 2.83 | 648 | 0.01 | 2020[32] |
| 29[a] |  | 530 | 3.27 | 635 | 0.18 | 2020[32] |
| 30[c] |  | 520 | 1.59 | 648 | N/A | 2020[40] |
| 31[c] |  | 570 | 2.05 | 736 | N/A | 2020[40] |

| Compound | Structure | | | | | |
|---|---|---|---|---|---|---|
| 32[c] | | 606 | 3.10 | 786 | N/A | 2020[40] |
| 33[a] | | 760 | 4.58 | 924 | <0.01 | 2020[35] |
| 34[a] | | 684 | 2.43 | 900 | <0.01 | 2020[35] |
| 35[d] | | 727 | 4.45 | 957 | 0.04 | 2022[36] |
| 36[d] | | 756 | 5.22 | 957 | 0.03 | 2022[36] |
| 37[d] | | 767 | 5.43 | 963 | 0.03 | 2022[36] |
| 38[d] | | 788 | 5.61 | 959 | 0.04 | 2022[36] |
| 39[d] | | 859 | 7.41 | 1004 | 0.03 | 2022[36] |
| 40[d] | | 746 | 5.61 | 950 | 0.03 | 2022[36] |
| 41[e] | | 768 | n.a. | 1034 | 0.01 | 2022[37] |
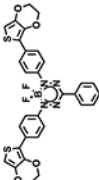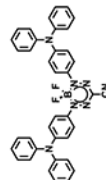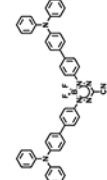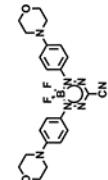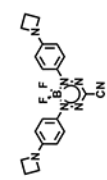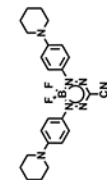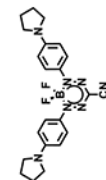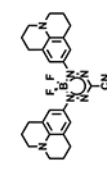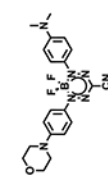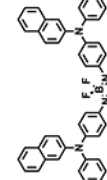
[a] Compounds were tested in CH2Cl2 solution.

[b] Compounds were tested in toluene solution.

[c] Compounds were tested in acetonitrile solution.

[d] Compounds were tested in DMSO solution.